# VIBRATIONAL DIAGNOSTICS AND ROTOR DYNAMICS OF CENTRIFUGAL COMPRESSORS IN ROTATING STALL

DONALD E. BENTLY
PAUL GOLDMAN
JING YUAN
*Bently Rotor Dynamics Research Corporation*
*1711 Orbit Way, Building 1*
*Minden, Nevada  89423, USA*

## Abstract

This paper discusses the rotating stall and surge in centrifugal compressors from the standpoint of vibrational diagnostics and rotor dynamics.  The literature survey shows insufficient understanding of rotor dynamic implications of rotating stall.  Most of the literature on the subject addresses only aerodynamic aspects of the problem, thus putting an empress on stall cells with exclusion of the rotor vibrational response. This paper treats a compressor as a coupled mechanical-aerodynamic system.  For the rotor/fluid system, the results of Dynamic Stiffness identification of an experimental centrifugal compressor in rotating stall and in normal operating conditions are presented.  It is shown that the aerodynamically induced radial (direct spring) stiffness coefficients are negative in normal operating conditions.  The negative radial stiffness effect in the case of rotating stall is even more profound.  The result of it that the rotor system mechanical resonance could be reduced as much as to 5-10% of running speed.  The conclusion is that the rotor dynamic stability margin during rotating stall is reduced.  As a conclusion from the overview of case histories and aerodynamic researches, a diagnostic strategy is suggested.

## 1.  Introduction

The interest in radial compressor fluid-induced instabilities started in the mid-seventies.  Since then, a number of case histories of high-pressure centrifugal compressor instabilities have been published [1-17].  Most of the publications report two types of rotor vibrational behavior: 1) High eccentricity and rotor first natural frequency re-excitation, 2) Subsynchronous forward precession with rotative speed dependent frequency.  The former is usually referred to as whip-type behavior and is normally associated with balance pistons, fluid film bearings, and labyrinth seals.  The latter is called whirl-type behavior [27-28] and can be associated either with fluid film bearings/seals or with rotating stall.  Rotating stall usually results in an appearance of a low subsynchronous frequency component in the rotor vibration spectrum (frequency ratios fall typically between 8 and 40 %, but can go as high as 80% of rotative speed [20]).  The emphasis on rotor behavior does not allow for details of particular flow patterns, but treats the fluid (gas) "in average," which falls in the scale of rotor motion.

## 2.  Case History

A 5-stage propylene compressor provides an example of the industrial centrifugal compressor behavior under the conditions of surge/rotating stall.  The orbits (Fig. 1) show a typical forward precession with frequency 0.15×, supported by the lateral vibration, half spectrum cascade data

(Fig. 2, the data was taken before full spectrum becomes available). The gas pressure measured at the outlet of the third stage is presented as a timebase waveform for the steady state regime (Fig. 3) and spectrum cascade plot for the startup (Fig. 4).
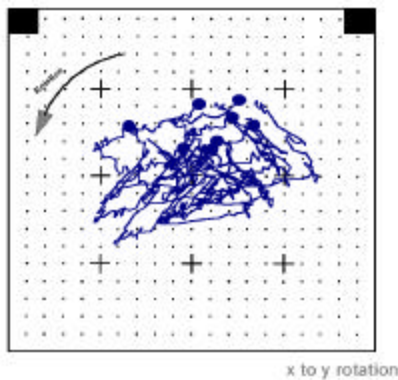


Figure 1. Typical orbits of the **lateral vibrations** of the rotor at the outboard bearing of a 5-stage propylene centrifugal compressor rotor in rotating stall conditions.
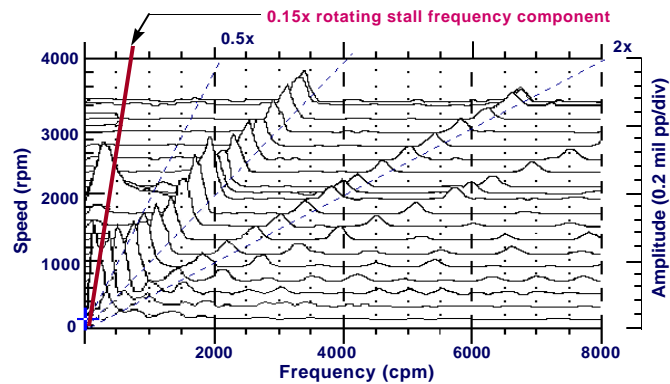


Figure 2. Half spectrum cascade plot of the **vertical lateral vibrations** of the rotor at the outboard bearing of the 5-stage propylene compressor during startup.
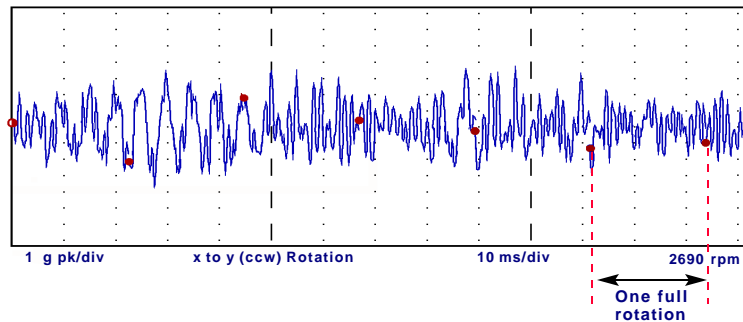


Figure 3. **Gas pressure oscillations** measured after the third stage of 5-stage propylene compressor in steady state regime. Note high vane passing frequency modulated by the low frequency of rotating stall/surge.
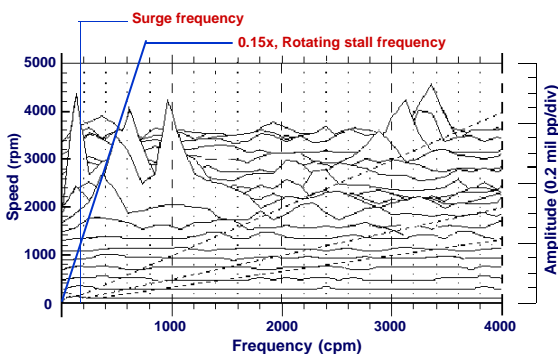


Figure 4. Half spectrum cascade plot of **gas pressure oscillations** at the outlet of the third stage of 5-stage propylene compressor during startup.
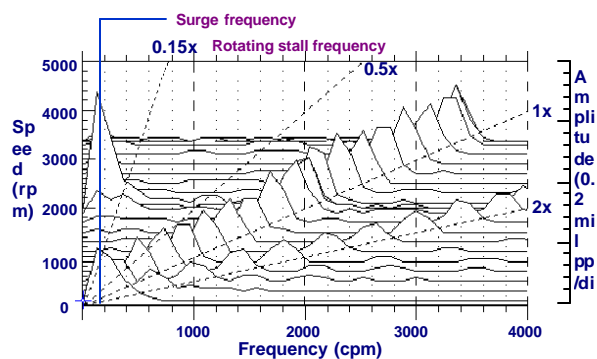


Figure 5. Half spectrum cascade plot of the **rotor axial vibrations** of the 5-stage propylene compressor during startup, showing surge component.

VIBRATIONAL DIAGNOSTICS AND ROTOR DYNAMICS OF CENTRIFUGAL
COMPRESSORS IN ROTATING STALL

The steady state data shows the combination of vane passing high frequency with low frequency oscillations. Using the spectrum cascade plot, the latter are identified as surge component (4.2 Hz) and rotating stall component (0.15×). It is important to note that the spectrum cascade of the thrust probe data (Fig. 5) shows a strong activity at the surge frequency, while the rotating stall component is much smaller. The described behavior is a reflection of the surge, which causes axial vibration at frequency 5 Hz at 2,000 rpm, while rotating stall is mainly causing forward circular radial vibration.

### 3. Instrumentation and Diagnostics Strategy

A typical machine train for a centrifugal compressor unit is shown in Fig. 6. It includes engine (in this case an aeroderivative gas turbine), gearbox, and the compressor itself. Different instrumentation setups for vibration, as well as performance diagnostics and monitoring of the engine, are beyond the scope of this paper. For the centrifugal compressor, the instrumentation package normally includes a Keyphasor® transducer, two sets of proximity probes in XY configuration installed at the inboard and outboard bearing locations (see Compressor DE and Compressor NDE in Fig. 6), two axial transducers, and performance monitoring instrumentation. As a minimum, the compressor performance monitoring instrumentation is supposed to include inlet and discharge pressure, temperature, and discharge flow measurements. Using the described instrumentation and case histories analysis, the rotating stall or surge can be identified based on the following information:
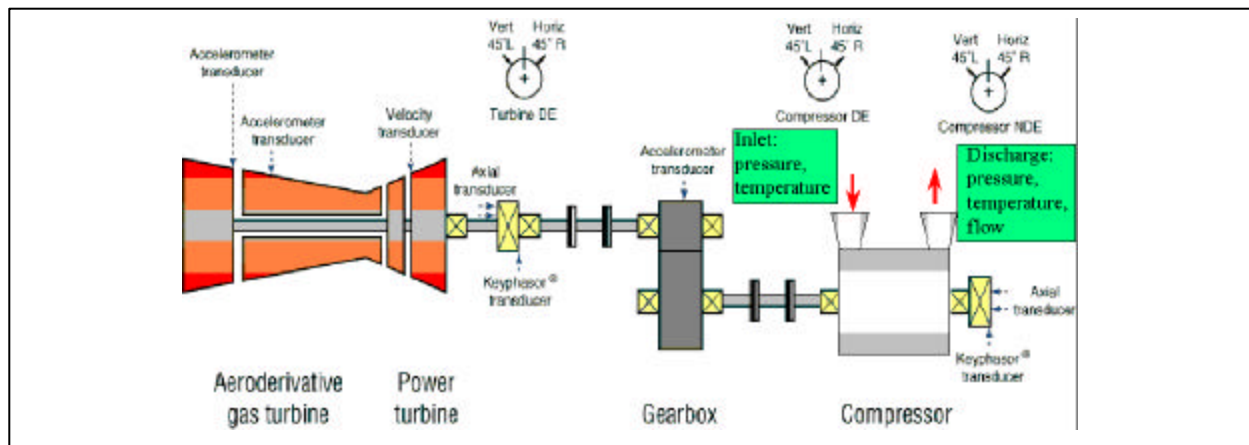


Figure 6. Typical compressor train diagram.

- **Radial vibration**
  Steady state data: direct orbits, full spectrum
  Indication: subsynchronous forward component
  Possible causes: **rotating stall**, fluid-induced instability, and surge
  Transient data: direct orbits, full spectrum cascade
  Indication: subsynchronous forward component with frequency proportional to the rotative speed (0.1 to 0.8×)
  Possible causes: **rotating stall**, fluid-induced instability
- **Axial vibration**
  Steady state data: spectrum

Indication:  subsynchronous component
Possible causes:  **rotating stall** (possible weak coupling) and **surge**
Transient data:  spectrum cascade
Indication:  subsynchronous component with low constant frequency
Possible causes:  **surge**

- **Pressure, temperature, and flow**
  Trend data:  (dc signal)
  Indication:  pressure head and flow decrease, temperature increases
  Possible causes:  **surge**, less likely rotating stall
  Note:  if pressure head and flow indicate a position on the performance curve close to the surge point, it could support rotating stall or surge versus fluid-induced instability.
  Dynamic data
  Indication:  vane passing frequency amplitude modulation of pressure, with constant flow
  Possible cause:  **rotating stall**
  Indication:  pressure vane passing frequency amplitude modulation with correlated flow oscillations
  Possible cause:  **surge**

As indicated above, a strong conclusion can only be reached by the correlation of vibration data with performance information.  It is important to note that rotating stall can originate in a particular stage of multistage compressor.  To localize the rotating stall source, additional pressure transducers may be required.

## 4.  Experimental Compressor for Rotating Stall

An experimental rig (Fig. 7) is constructed to evaluate Dynamic Stiffness for the rotor/fluid system during rotating stall and normal operating conditions.  The rig consists of a single stage centrifugal compressor with a vaneless diffuser, driven by a 1-hp dc electric motor.  The motor speed is controlled by a high-output, variable power supply, and the speed can be controlled from near zero to 17,000 rpm.  The motor is attached to the compressor rotor by a flexible disk coupling.
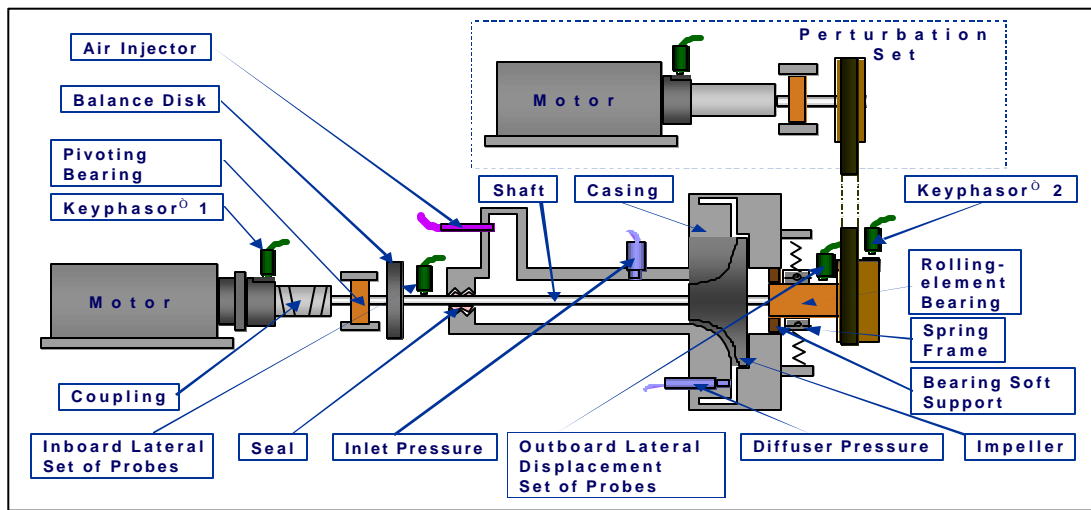


Figure 7.  Experimental compressor setup.

## VIBRATIONAL DIAGNOSTICS AND ROTOR DYNAMICS OF CENTRIFUGAL COMPRESSORS IN ROTATING STALL

The compressor rotor is separated into two pieces: a rotating section from the motor to the outboard end of the compressor and a nonrotating stub shaft from the outboard compressor bearing to the outermost support bearing. The rotating section is supported by two bearings: a pivoting bearing on driver-end and a rolling-element bearing on the nondriver-end in a soft support. A spring-load frame is attached to the nondriver-end of nonrotating stub shaft to control the radial position of the compressor rotor and counteract the gravity load of the rotor. The nonrotating stub shaft also provides the input for the perturbation set. The nonsynchronous perturbator transmits an exciting rotating force with variable frequency to the compressor rotor with a constant rotating force, 1.3 N.

Two orthogonal pairs of eddy current displacement transducers are mounted next to the inboard bearing and at the spring-load frame to measure the displacement of the rotor. Two Keyphasor® probes are installed on the compressor shaft and the perturbator disk to provide phase and speed references. A conical exhaust valve on a lead screw controls airflow through the compressor. The valve is located at the end of the discharge pipe from the compressor (not shown in Fig. 7). It can be adjusted by several turns from fully closed, which completely blocks the output flow of the compressor. When the valve is fully opened, the airflow passes with minimum restriction. The actual flow is monitored by a flowmeter. Dynamic pressure transducers measure the compressor inlet and discharge pressure, as well as pressure wave propagation in the diffuser (at the same radius, 90° apart).

### 4.1.    Compressor performance

An experimental compressor performance chart is displayed in Fig. 8 nondimensionally, applying general conversion rules as [27].

As it can be observed in Fig. 8 that with the airflow increase, the pressure drops, and the compressor is out of the rotating stall regime. Increase of the airflow stabilizes the compressor. The phenomena is supported by the full spectrum waterfall data, Fig. 9, taken at a constant rotative speed with the flow increasing by opening the exhaust value from full close to wide open.
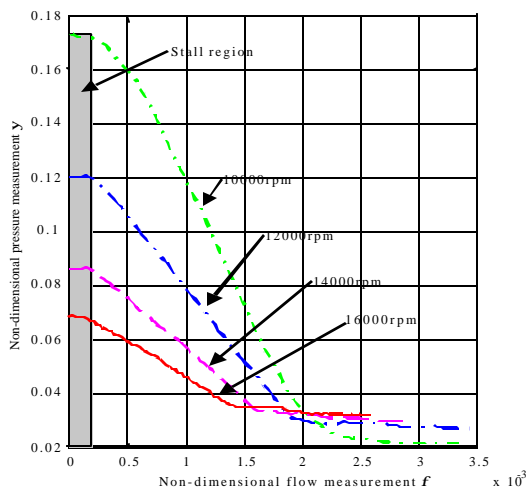


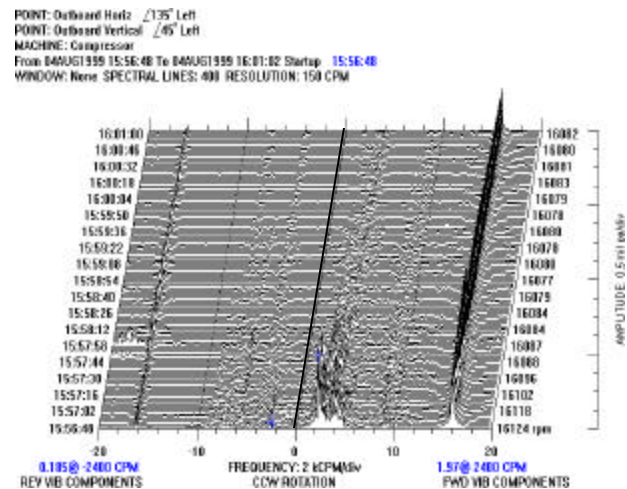Figure 8. **Differential pressure** (outlet subtract inlet) versus airflow.



Figure 9. Waterfall plot generated from the outboard **lateral vibration** data with increasing airflow.

## 4.2. Rotating stall experiments of compressor startups

Under the flow constriction conditions, the experimental compressor rotor exhibits rotating stall whirl with a subsynchronous frequency component of 0.15× in the forward direction, presented in Figs. 10 to 12. Compared to the field case history above, the orbits (Fig. 10) show a clear forward precession with frequency 0.15×, supported by full spectrum cascade data (Fig. 11) generated from the lateral vibration. In addition, full spectrum cascade data (Fig. 12) is generated from pressure transducers, mounted in diffuser, further substantiating this result.
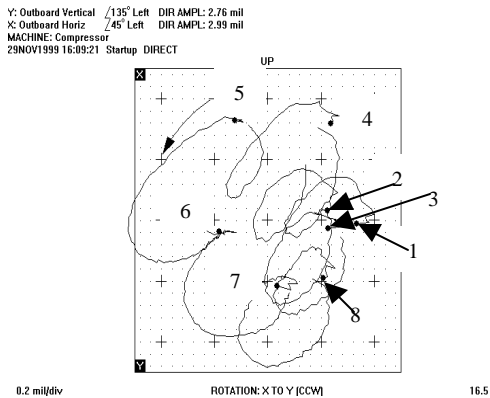


Figure 10. Direct orbit plot of the outboard **lateral vibration** data in rotating stall operating conditions. 1-8 are consequent Keyphasor numbers.
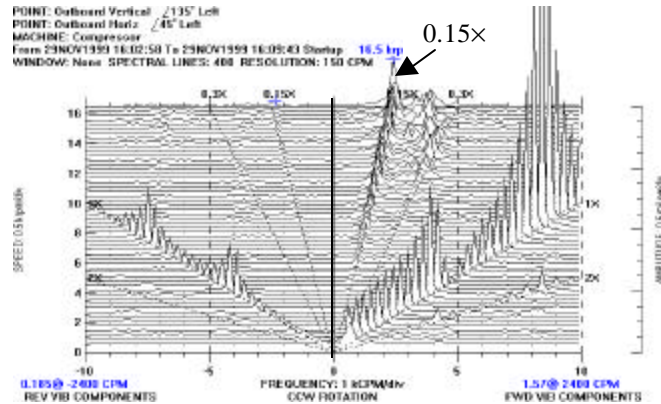


Figure 11. Full spectrum cascade plot of the outboard **lateral vibration** data in rotating stall operating conditions.
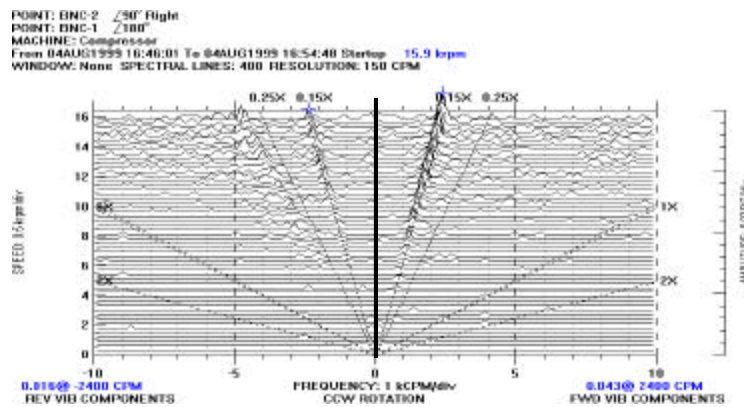


Figure 12. Full spectrum cascade plot generated from **diffuser pressure** transducers, positioned 90° apart, in rotating stall operating conditions.

## 4.3. Nonsynchronous perturbation tests

A series of nonsynchronous perturbation tests are performed at each of four compressor running speeds: 10,000, 12,000, 14,000, and 16,000 rpm. For the detailed description of the applied methodology see [29]. At each running speed, perturbation runs are performed under two different valve positions, chosen as close to each other as possible or more opened up for two values of mess flow. Those valve positions provide rotating stall operation or normal operation conditions respectively. The perturbator generates a force of magnitude $F$ with orientation $\boldsymbol{d}$ rotating in the same direction as the compressor rotation (forward perturbation), resulting in the perturbation vector $Fe^{jd}$. The perturbator is revved up from slow roll speed to 5,000 rpm in

# VIBRATIONAL DIAGNOSTICS AND ROTOR DYNAMICS OF CENTRIFUGAL COMPRESSORS IN ROTATING STALL

order to identify Dynamic Stiffness of the rotor first mode. The vibration signals from two orthogonal, eddy current displacement transducers located at spring-load frame as 45° (*x*) and 135° (*y*) to the left (as seen from the driver) are filtered to the frequency **w** of the perturbation force. This yields amplitudes and phases for vertical (*y*) and horizontal (*x*) components of the response.

In order to minimize the influence of mechanical stiffness asymmetry, 1× vertical $\vec{Y}_w$ and horizontal $\vec{X}_w$ vectors are combined into the circular forward (in the direction of perturbation) component:

$$\vec{A}_\omega^{(fwd)} = \vec{Y}_\omega + j\vec{X}_\omega \tag{1}$$

Next, the perturbation process is repeated for the perturbation in a direction opposite the rotation of the compressor rotor (reverse perturbation) for each running speed **W** and valve settings. In this case, the forward (in the direction of perturbation) component of the filtered-to-perturbation-frequency response is opposite the direction of rotation. The nonsynchronous Dynamic Stiffness is calculated by taking the ratio of the force input to the response vectors for each speed in the databases.

$$DS(\textbf{\textit{w}}) = DDS(\textbf{\textit{w}}) + jQDS(\textbf{\textit{w}}) = \frac{Fe^{jd}}{\vec{A}_w^{(fwd)}}, \quad DDS(\textbf{\textit{w}}) = direct(DS), \quad QDS(\textbf{\textit{w}}) = quad(DS) \tag{2}$$

Figures 13 and 14 present the forward and reverse perturbation data with the results of Dynamic Stiffness under the test conditions described above. The negative speed there corresponds to the reverse perturbation.
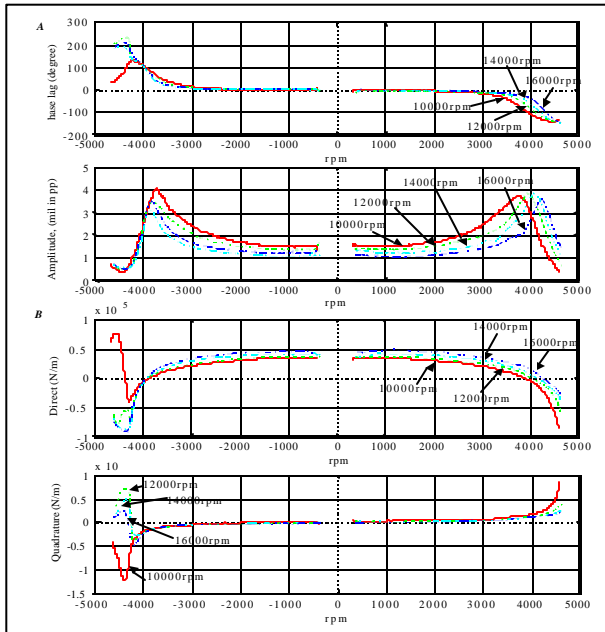


Figure 13. Forward and reverse perturbation data generated in **normal** operating conditions. *A)* response phases and amplitudes of the rotor outboard lateral. *B)* direct and quadrature Dynamic Stiffnesses.
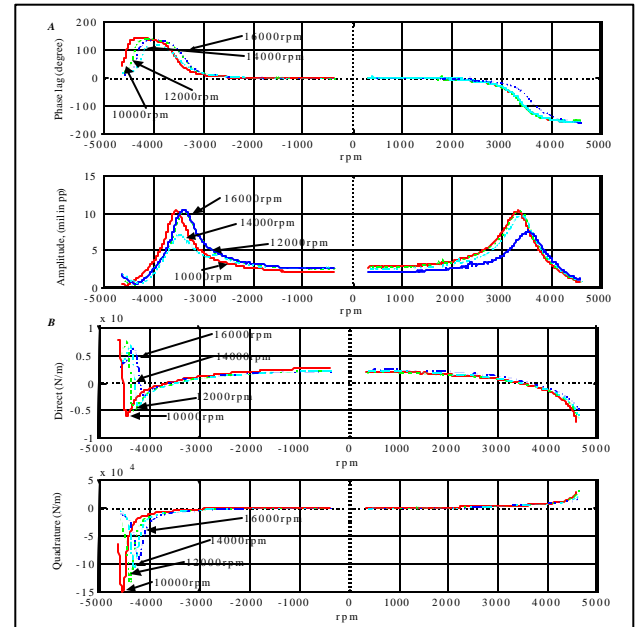
Figure 14. Forward and reverse perturbation data generated in **rotating stall** operating conditions. *A)* response phases and amplitudes of the rotor outboard lateral. *B)* direct and quadrature Dynamic Stiffnesses.

DONALD E. BENTLY

Both figures show that in the forward direction, the direct Dynamic Stiffness increases with the rotor speed increases, but in the reverse direction, the direct Dynamic Stiffness keeps about the same values for all rotor speeds. This phenomenon indicates the effect of the fluid inertia.

Since the total Dynamic Stiffness of the compressor consists of mechanical and aerodynamic parts, the former is measured by running nonsynchronous perturbation on the compressor at zero rotative speed ($DS_0$). The difference of Dynamic Stiffness between the running compressor and stopped compressor represents aerodynamically induced Dynamic Stiffness, $DS_{air}$:

$$DDS_{air}(w) = direct(DS - DS_0) = K_{air} - M_{air1}w^2 - M_{air2}(w - \mathbf{l}\Omega)^2$$
$$QDS_{air}(w) = quad(DS - DS_0) = D_{air}(w - \mathbf{l}\Omega)$$

(3)

where $M_{air1}$, $K_{air}$, $D_{air}$ are air inertia, radial stiffness, and damping respectively, generated by the air/impeller interaction. $M_{air2}$ is a fluidic mass effect term, and $\mathbf{l}$ represents a swirling ratio coefficient.

Equation (3) shows the parameters of direct and quadrature Dynamic Stiffness extrapolation. The results of the raw data and the described processed data are illustrated in Figs. 15 and 16. Figure 15 shows the reductions of air-induced radial stiffness. The swirling ratio coefficient $\mathbf{l}$ is shown in Fig. 16. The negative value of $\mathbf{l}$ indicates the reverse-flow pattern rotation. It gets stronger at lower rotor rotative speed and in the rotating stall operating conditions.
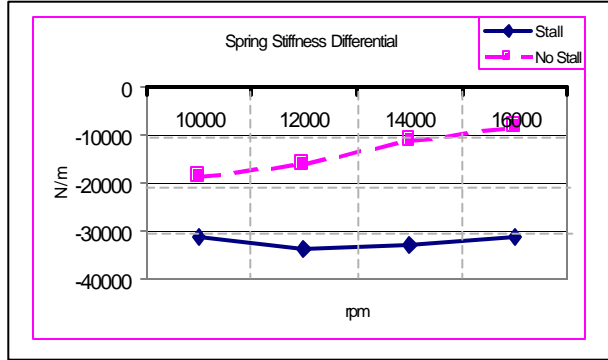


Figure 15. Air-induced **radial stiffness** calculated in rotating stall and normal conditions with rotative speed changes.
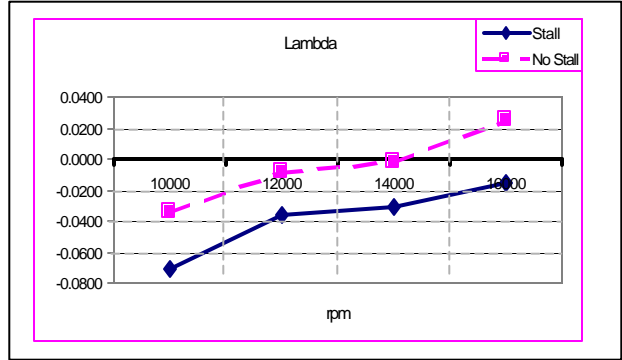


Figure 16. Swirling ratio coefficient $\mathbf{l}$ in rotating stall and normal conditions with rotative speed changes.
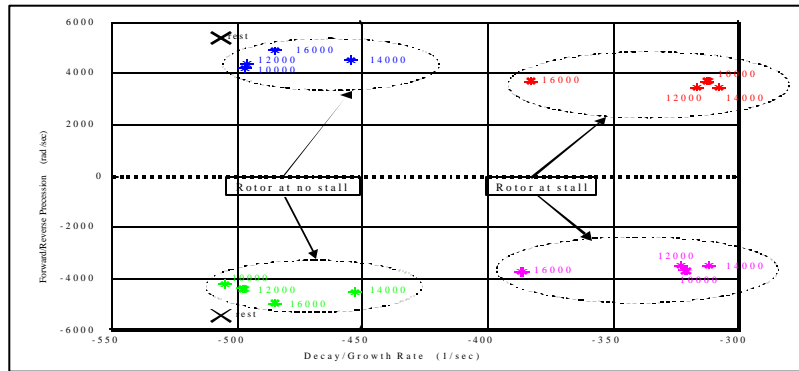


Figure 17. Eigenvalues for rotor in rotating stall and normal conditions comparing to mechanical model.

VIBRATIONAL DIAGNOSTICS AND ROTOR DYNAMICS OF CENTRIFUGAL
COMPRESSORS IN ROTATING STALL

Equation (3) allows also performing eigenvalue calculations for the compressor rotor dynamic stability evaluation, shown in Fig. 17. The eigenvalue analysis clearly shows that the rotating stall lowers radial stiffness and decay rates. In the case of rotating stall, increase of the rotative speed increases the rotor stability margin. The result of eigenvalue analysis shows that rotating stall not only lowers the rotor radial stiffness, but also brings the compressor toward the edge of the instability. (In the Fig. 17, the negative frequencies indicate the reverse perturbation).

Another set of perturbation tests is performed for increased the airflow of the compressor. The tests also include forward and reverse perturbations with two rotative speeds of the compressor rotor. In order to produce the Dynamic Stiffness (Fig. 18-B) from the perturbation data (Fig. 18-A), the same routine is used as Eqs. (1) and (2). The same concept of subtracting the mechanical Dynamic Stiffness from total Dynamic Stiffness (Eq. (3)) is used to determine the aerodynamic part of Dynamic Stiffness. The results are illustrated in Figs. 19 and 20. They show that the airflow increases the direct Dynamic Stiffness (Fig. 18). This offsets the negative effect of the radial stiffness induced aerodynamically (Fig. 19). The swirling ratio coefficient *l* becomes positive as the airflow increases (Fig. 20). Figure 21 shows the result of the corresponding eigenvalue calculations, showing that when the airflow gets stronger, the compressor moves away from rotating stall regime and becomes more stable.
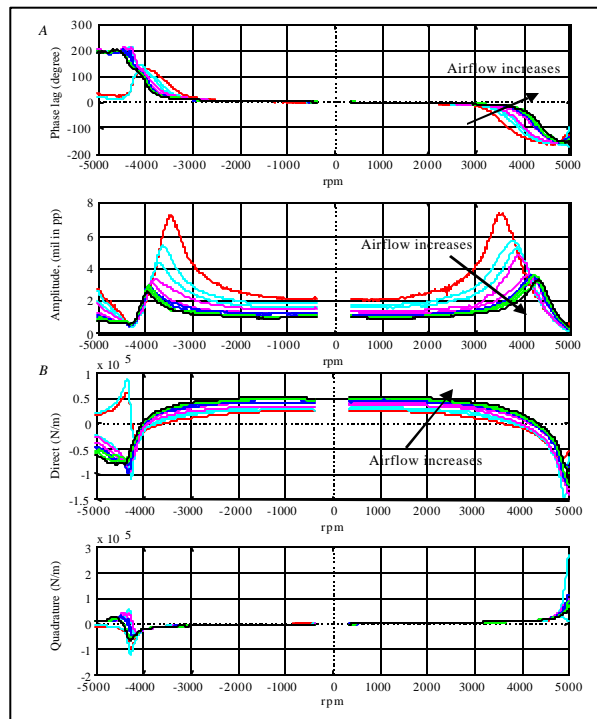


Figure 18. Forward and reverse perturbation data generated in rotating stall conditions at rotative speed 16,000 rpm. *A*) lateral response phase and amplitude at the rotor outboard. *B*) direct and quadrature Dynamic Stiffnesses.
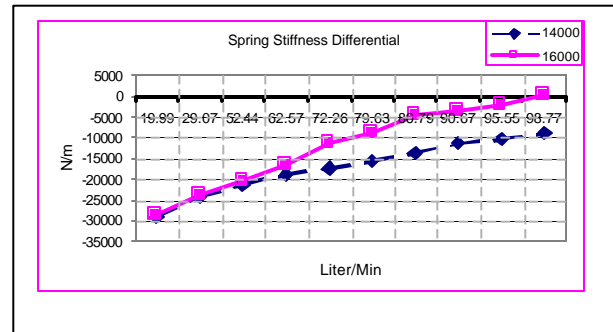


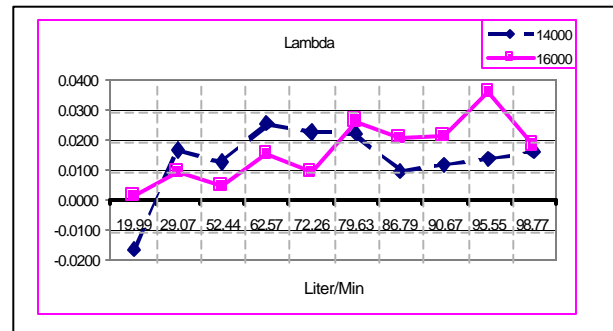Figure 19. Air-induced **radial stiffness** calculated with airflow changes for deferent rotative speed.



Figure 20. Swirling ratio coefficient *l* calculated with airflow changes for deferent rotative speed.
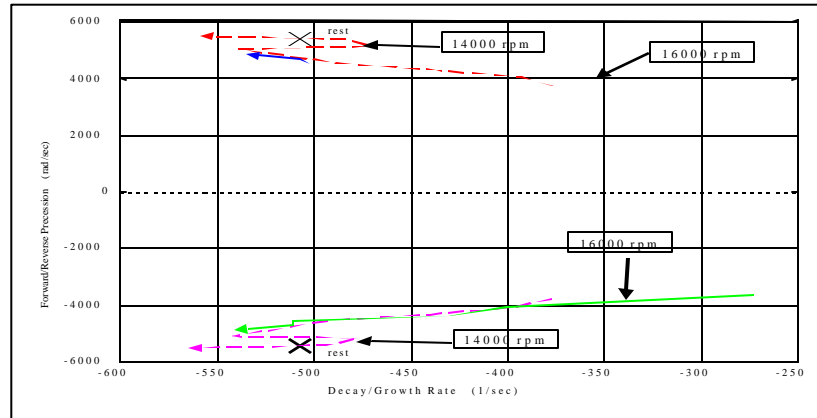
Figure 21.  Eigenvalues at two rotor rotative speeds with airflow changes.

## 5.  Conclusions

This paper provides some practical recommendations on the rotating stall diagnostics as well as some insight into rotor dynamic implications of the phenomenon.  It fills the gap in the literature on rotating stall, which all but ignore the rotor dynamic implication of rotating stall.  The most significant conclusion from this paper is that aerodynamic forces applied to the impeller generate negative radial stiffness (stiffness $K_{air}$ appears negative in all experiments).  It is also important that this stiffness drops even more during the rotating stall.  In short, the conclusions can be formulated as follows:

- The rotating stall conditions manifest in the rotor lateral vibration signature as rotor forward precession with subsynchronous frequency, which tracks the rotor speed.  This behavior is referred as a rotating stall whirl.
- From the diagnostic standpoint, rotating stall differs from other instabilities of the whirl type in its strong dependence on the compressor operating conditions; it should disappear with increased flow.  It differs from surge by its frequency proportionality to the rotative speed as well as by the predominantly axial character of surge-caused vibrations.
- Surge conditions manifest in the rotor response as predominantly axial vibrations with low frequency independent of rotative speed.
- The parameter clearly identified by nonsynchronous perturbation tests is aerodynamically induced radial stiffness.  In all conditions, it is negative.  From the practical standpoint, it means that even in normal operation conditions, centrifugal compressors have lower natural frequencies than it appears in purely mechanical calculations.
- The aerodynamically induced radial stiffness during rotating stall drops dramatically and ultimately can make a compressor unstable.  The data from field case histories indicates that the resulting mechanical resonance can be driven by rotating stall as low as 5-10% of running speed.
- Altogether, aerodynamic forces may have a significant destabilizing effect on the compressor.  In the case of a flexible rotor and/or soft bearings, they are able to create a rotor dynamic instability of whirl type.

VIBRATIONAL DIAGNOSTICS AND ROTOR DYNAMICS OF CENTRIFUGAL
COMPRESSORS IN ROTATING STALL

**Reference**

1.  Fowlie, D. W., Miles, D. D., (1975) "Vibration Problems With High Pressure Centrifugal Compressors," ASME 75-Pet-28, Petroleum Mechanical Engrg. Conf., Tulsa, Oklahoma.
2.  Smith, K. J., (1975) "An Operation History of Fractional Frequency Whirl," Proceedings of 4th Turbomachinery Symposium.
3.  Wachel, J. C., (1975) "Nonsynchronous Instability of Centrifugal Compressors," ASME 75-Pet-22.
4.  Ferrara, P., (1977) "Vibrations in Very High Pressure Centrifugal Compressors," ASME 77-Det-15.
5.  Kaneki, T., Eino, T., (1979) "Centrifugal Compressor for Urea Synthesis Plant," Hitachi Review, Vol. 28, No. 6.
6.  Ek, M. C., (1978) "Solution of the Subsynchronous Whirl Problem in the High Pressure Hydrogen Turbomachinery of the Space Shuttle Main Engine," AIAA/SAE 14th Joint Propulsion Conference, Las Vegas, Nevada.
7.  Geary, C. H., Damratowsky, L. P., Seyer, C., (1976) "Design and Operation of the World's Highest Pressure Gas Injection Centrifugal Compressor," No. 0TC 2485, presented at the Offshore Technology Conference, Houston, Texas.
8.  Sabella, D., Terrinoni, L., Timori, A., (1981) "Full Load Testing of Centrifugal Natural Gas Injection Compressors," Inst. Mech. Ing. Conference Publications.
9.  Coletti, N. J., Crane, M. E., (1981) "Centrifugal Compression on the Arun High Pressure Injection Project," Inst. Mech. Ing. Conference Publications.
10. Bonciany, L., Ferrara, P. L., Timori, A., (1980) "Aero-Induced Vibrations in Centrifugal Compressors," Workshop on Rotordynamic Instability at Texas A&M University, Texas.
11. Bonciani, L., Terrinoni, L., Tesei, A., (1982) "Unsteady Flow Phenomena in Industrial Compressor Stage," NASA Conference Publication 2250.
12. Excerpts From Turbomachinery Technology Seminar, 11-14 March 1984, Coronado, California.
13. Wendt, P. G., (1985) "Forced Low Frequency Vibration Due to Aerodynamic Flow Instability (Rotating Stall)," Solar Turbines, Inc., Engineering Report 2832.
14. Fulton, J. W., (1986) "Subsynchronous Vibration of a Multistage Centrifugal Compressor Forced by Rotating Stall," Turbomachinery Technology Seminar 1986, Solar Turbines, Inc., San Diego, California, February.
15. Emmons, H. W., Pearson, C. E., Grant, H. P., (1955) "Compressor Surge and Stall Propagation," Trans. ASME, Vol. 79.
16. Lennemann, E., Howard, J. H. G., (1970) "Unsteady Flow Phenomena in Rotating Centrifugal Impeller Passages," ASME 69-GT-35, ASME Journal of Engrg. for Power, Vol. 108.
17. Frigne, P., Van den Braembusse, R., (1984) "Distinction Between Different Types of Impeller and Diffuser Rotating Stall in a Centrifugal Compressor With Vaneless Diffuser," ASME Journal of Engrg. for Gas Turbines and Power, Vol. 106, No. 2.
18. Van den Braembusse, R., (1987) "Rotating Stall in Centrifugal Compressors," von Karman Institute for Fluid Dynamics, Preprint, Belgium.
19. Haupt, U., Seidel, U., Abdel-Hamid, A. N., Rautenberg, M., "(1988) Unsteady Flow in a Centrifugal Compressor With Different Types of Vaned Diffusers," ASME 88-GT-22.

DONALD E. BENTLY

20. Jin, D., Haupt, U., Hasemann, H., Rautenberg, M., (1992) "Blade Excitation by Circumferentially Asymmetric Rotating Stall in Centrifugal Compressors," ASME 92-GT-148.

21. Chen, J., Huang, X., Hasemann, H., Seidel, U., Jin, D., Rautenberg, M., (1993) "The Interpretation of Internal Pressure Patterns of Rotating Stall in Centrifugal Compressor Impellers," ASME 93-GT-192.

22. Tsujimoto, Y., Acosta, A. J., (1987) "Theoretical Study of Impeller and/or Diffuser Attributed Rotating Stalls and Their Effects on Whirling Instability of a Centrifugal Impeller," Work Group of Hydraulic Machinery Under Steady Oscillatory Conditions, Lille, France.

23. Pampreen, R. C., (1993) "Compressor Surge and Stall," Concepts ETI, Inc., Norwich, Vermont.

24. Bently, D. E., Muszynska, A., (1988) "Role of Circumferential Flow in the Stability of Fluid-Handling Machine Rotors," The 5th Workshop on Rotordynamic Instability Problems in High Performance Turbomachinery, Texas A&M University, College Station, Texas, NASA CP 3026.

25. Muszynska, A., Bently, D. E., (1990) "Frequency Swept Rotating Input Perturbation Techniques and Identification of the Fluid Force Models in Rotor/Bearing/Seal Systems and Fluid-Handling Machines," Journal of Sound and Vibration, Vol. 143, No. 1.

26. Colding-Jorgensen, J., (1993) "Rotordynamic Effects of Impeller Flow in Centrifugal Compressors," VDI Bevichte, No. 1082.

27. Bently, D. E., Goldman, P., (1998) "Destabilizing Effect of Aerodynamic Forces in Centrifugal Compressors," ISROMAC-7, Honolulu, Hawaii.

28. Sorokes, J. M., Marshall D. F., (1998) "A Review of Aerodynamically Induced Forces Acting on Centrifugal Compressors, and Resulting Vibration Characteristics of Rotors," Proceedings of the 27th Turbomachinery Symposium, Texas A&M.

29. Bently, D. E., Goldman, P., (2000) "Vibrational Diagnostics of Rotating Stall in Centrifugal Compressors," Orbit, BNC, Vol. 21 No 1.